

## Design and Control of a Permanent Magnet Assisted Synchronous Reluctance Motor

Loubna Boudjelida<sup>1,2</sup>, Cagdas Hisar<sup>3\*</sup> and Ibrahim Sefa<sup>2</sup>

0009-0006-4218-062X, 0000-0001-8278-3501, 0000-0002-2093-683X

<sup>1</sup> Department of Electrical Engineering, Faculty of Technology sciences, Constantine1 University, Algeria

<sup>2</sup> Department of Electrical and Electronics Engineering, Faculty of Technology, Gazi University, Ankara, 06500, Turkey

<sup>3</sup> Department of Automotive Engineering, Faculty of Technology, Gazi University, Ankara, 06500, Turkey

### Abstract

In recent years, studies aiming to use different motor types for traction purpose, such as in electric vehicles, have become increasingly widespread. Among these motor types, permanent magnet assisted synchronous reluctance motor has become increasingly preferred in commercially electric vehicles nowadays. This study addresses the design and control of a permanent magnet assisted synchronous reluctance motor, also the comparison with the synchronous reluctance motor. The motor design process is carried out using the finite element method in Ansys-Maxwell environment. A series of a simulation studies is conducted in the MATLAB/Simulink environment for controlling the obtained motor designed in Ansys-Maxwell. The field-oriented control approach is chosen for precise speed control. As a result of the simulation studies, it is observed that the designed motor tracks the reference with minimal error under various load conditions within a closed-loop system. Also, this paper investigates how the permanent magnet implementation affects the machine performance comparing to synchronous reluctance motors. In addition, such a study takes into account that the design of machines involves always several constraints, including geometry, materials, supply limits, and performance constraints.

Keywords: Field Oriented Control; Finite Element Method; Permanent Magnet Assisted Synchronous Reluctance Motor; Synchronous Reluctance Motor; Traction Motor.

### Research Article

<https://doi.org/10.30939/ijastech.1366882>

Received 26.09.2023

Revised 05.11.2023

Accepted 15.11.2023

\* Corresponding author

Cagdas Hisar

[chisar@gazi.edu.tr](mailto:chisar@gazi.edu.tr)

Address: Department of Automotive

Engineering, Faculty of Technology,

Gazi University, Ankara, Turkey

Tel:+903122028661

## 1. Introduction

Automotive applications focus on developing drive-motor technologies with high energy efficiency and low environmental impact. Electric and hybrid vehicles are gaining popularity since they satisfy these conditions [1,2]. Amongst the most relevant electric motors used in traction applications, rare-earth-based permanent magnet synchronous motors (PMSMs) are very common due to their robustness in terms of specific power, speed range capability, and efficiency [3,4]. Although, a lot of studies concerning rare-earth permanent magnet (PM) materials, such as high price and material rarity, are interested in using other alternatives as ferrite magnets [5,6]. In [7] a five phase external rotor permanent magnet assisted synchronous reluctance motor (PMA-SynRM) has been designed for rare earth based neodymium (Nd) rotor and ferrite based (Fe) rotor. The results compared both rotor type and showed that ferrite PMs increased the input current and decreased torque pulsations. For this reason, PMA-SynRMs are becoming very popular nowadays since they combine both the advantages of PMSMs and the low manufacturing costs of induction motors [8,9]. PMA-SynRM motors have various applications in different fields, such

as industrial drives, renewable energy systems, and electrical vehicles (EVs) [10,11].

PMA-SynRM is a type of AC synchronous motor that combines the structure characteristics of synchronous reluctance motors (SynRMs) and PMSMs [12]. Its rotor contains flux barriers inserted by PMs. The rotor produces a magnetic field that interacts with the rotating magnetic field of the stator, generating torque. The torque depends on both the PM and the reluctance effects. In [13] a combination of both benefits of PMA-SynRM and internal PMSM (IPMSM) was investigated by designing a modified PMA-SynRM rotor structure. This type motor produces high smooth output torque and needs less PMs.

Adding to the challenges associated with the PMA-SynRM, the inserted PMs offers a lot of different rotor shapes that can be investigated in the future. The rotor flux barriers can be optimized as well as the placement and orientation of PMs. A novel topology using V-shape PMs is used in [12] to improve torque characteristics. The idea is to insert PMs in the rotor where they can provide maximum torque. According to the results, the average torque is increased 53%, and ripples are decreased by 65%. In [14] PM optimization was investigated for four different designs, where the

optimal solution presented significantly high PF and torque with acceptable torque ripples. Furthermore, the comparison of this type of motor with IPMSMs is very interesting since they are popular among EV motors due to their rotor similarity, robustness, and high quality performances.

Literally, synchronous machines with field winding can be easily controlled by field currents but their efficiency is often lower because of the increase in field copper losses [15,16]; whereas PM synchronous machines are difficult to control and expensive, also can provide PM demagnetization at high temperatures [17]. PMA-SynRM is considered one of the best solutions, it offers great mechanical robustness in terms of protection of PMs versus the centrifugal force, and it can produce a large reluctance torque to maintain the power density and reduces irreversible demagnetization risk [18]. However, the additional PM flux in the d-axis direction raises the back electromotive force (EMF), thus torque density, power factor (PF), and efficiency of the PMA-SynRM should be improved. The complexity of rotor design and manufacturing are considered as drawbacks of these types of motors [19,20].

PMA-SynRM motors are controlled and regulated by using a position sensor and a suitable control strategy [21]. The position sensor can be either a resolver, an encoder, or a hall sensor, depending on the accuracy and robustness required. The control strategy can be a vector control or direct torque control [22], depending on the speed range and dynamic performance required. Vector control is a method that decouples the torque and flux components of the stator current by using a coordinate transformation. This allows the control of the motor torque and speed independently. Vector control can be implemented with field-oriented control (FOC) or direct torque control (DTC) [23,24]. Direct torque control is a method that directly controls the stator flux and torque by selecting the optimal voltage vector from a switching table. This eliminates the need for coordinate transformation and current regulators. DTC can be implemented with hysteresis modulation or space vector modulation (SVM). On the other hand, FOC involves transformations to switch the reference frame from a natural reference frame to a synchronous reference frame and calculates d and q-axis parameters for every cycle [25]. These transformations require trigonometric functions that come with a calculation burden. Although implementing FOC is more complex, it provides more precise control.

In electrical machines, the operation of the rotor is based on the electromagnetic concept. Therefore, the electromagnetic design topology is very critical in order to analyze the motor performances, such as electromagnetic torque, output power and efficiency [12,26]. This design proposes the calculation of motor parameters such as rotor torque, power losses, and power factor. On the other hand, the analysis of flux density, saturation and motor vibration is necessary before the construction of any motor. In order to get the magnetic field, three different methods of analysis are existing, magnetic circuit method, analytical model, and finite element method (FEM) that will be used in this work.

Many studies have been carried out in the field of designing PMA-SynRM rotors, where it is possible to improve the output

torque and the power factor by increasing d-q axis inductance difference ( $L_d - L_q$ ) and the saliency ratio ( $L_d/L_q$ ) [27]. In this kind of motors, the most frequent configurations of the stator windings are distributed and concentrated slots windings [28,29]. Also, single- and double-layer windings focused to reduce harmonics [30]. The double layer topology eliminates the odd harmonics. Where, in single layer topology, the fundamental torque component is higher than the double layer topology. All these analyses should be taken into consideration to select the stator winding type for each application of the PMA-SynRM [30].

The contribution of this study is to investigate the dynamic performance of a PMA-SynRM designed by FEM in a simulation environment. In this study, the designed PMA-SynRM will be controlled using FOC technique, which allows the independent control of torque and flux of the motor. The coordinate transformation converts the stator currents from a stationary reference frame (abc) to a rotating reference frame (d-q) that is aligned with the rotor flux. The flux is controlled by d-axis current, while the electromagnetic torque is controlled by q-axis current. The FOC technique needs a position sensor in order to measure the rotor angle and two current regulators to control the d-axis and q-axis currents.

In the future sections it is necessary to find optimum parameters of the rotor flux barriers of the SynRM first, where this structure will be considered as a reference design. Secondly, the implementation of PMs will be carried out in the rotor of the proposed PMA-SynRM. The finite element results will be presented and compare both motor structures. Finally, a FOC controller is given using MATLAB/Simulink platform to improve the PMA-SynRM mathematical model.

## 2. Mathematical Modeling of PMA-SynRM/Drive System

The mathematical model of the PMA-SynRM is similar to that of the wound rotor synchronous motor except that the excitation winding does not exist [31]. In literature valid mathematical models for the instantaneous variation of voltage and current describing the performance of synchronous motor in both steady state and transient are generally obtained by the utilization of vector diagram theory shown in Fig. 1. This diagram shows all the necessary vectors to define the total flux linkage  $\Psi$  obtained by the PMA-SynRM.  $V_s$  and  $I_s$  represent the resultant stator voltage and current, respectively. Where  $\Psi_{PM}$  is the flux linkage generated by the inserted PMs which is aligned with the q-axis in the opposite

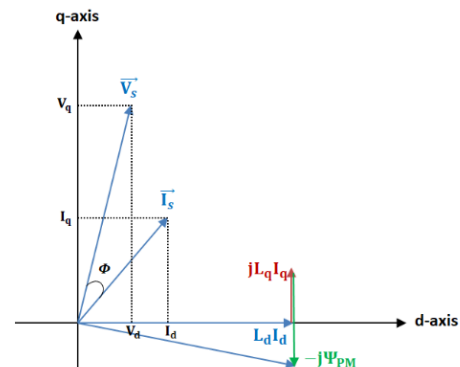


Fig. 1. Vector diagram in the synchronous reference frame

direction.  $\Phi$  is the angle between the stator voltage and current. It is noticed that the power factor angle  $\Phi$  is not high, which leads to a high PF compared to the PF of the SynRM.

Voltage equations of the PMA-SynRM in dq frame are expressed as follows:

$$v_d = R_s i_d + \frac{d\psi_d}{dt} - \omega_e \psi_q \tag{1}$$

$$v_q = R_s i_q + \frac{d\psi_q}{dt} - \omega_e \psi_d$$

Where:  $R_s$ ,  $i_d$ ,  $i_q$ ,  $\psi_d$ ,  $\psi_q$  are the stator resistance, d and q axis currents, and d and q axis flux linkages, respectively.

$$\omega_e = n_p \omega_m \tag{2}$$

$\omega_e$ ,  $\omega_m$ ,  $n_p$ , are electrical angular frequency, mechanical angular frequency, and number of pole pairs respectively. The flux linkage equations are:

$$\psi_d = L_d i_d \tag{3}$$

$$\psi_q = L_q i_q - \psi_{PM}$$

The electromagnetic torque is expressed as follows:

$$T_e = n_p i_d \left( (L_d - L_q) i_q + \psi_{PM} \right) \tag{4}$$

$L_d$ ,  $L_q$  are d and q-axis inductances,  $T_e$  is the produced electromagnetic torque.

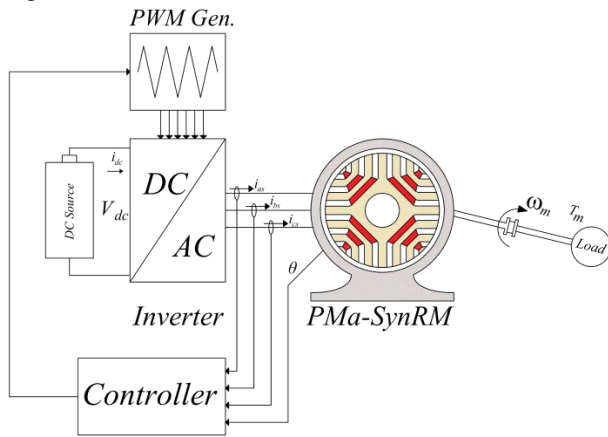


Fig. 2. A three phase PMA-SynRM drive prototype.

The PMA-SynRM and PMSM electromagnetic torques consist of reluctant torque and PM torque. However, in PMA-SynRM, the reluctant torque has the major driving role due to the substantial-disparity between  $L_d$  and  $L_q$  inductances. The expression of the mechanical dynamic equation of the PMA-SynRM is as follows:

$$J \frac{d\omega_m}{dt} = T_e - B_f \omega_m - T_L \tag{5}$$

Where  $J$  is the moment of inertia,  $B_f$  is the viscosity, and  $T_L$  is the load torque.

Recently, the development in machine design and power electronics enable motor designers to eliminate the starting rotor cage and get better performance using FOC controller [32,33]. Fig. 2 illustrates the AC three-phase inverter which supply the PMA-SynRM by symmetric sinusoidal three-phase voltages.  $V_{dc}$ ,  $i_{dc}$ ,  $i_{as}$ ,  $i_{bs}$ , and  $i_{cs}$  are the DC grid input voltage, the inverter current, and the load motor phase currents, respectively.

### 3. Finite Element Method of the Proposed Motors

FEM is the most used tool in motor design field, it is able to make preliminary decisions and process the design model. Fig. 3 represents the flowchart of the design steps used in this study. In the preprocessing part, it is necessary to define the different materials and geometries of each part of the motor. Also, the various performance parameters of the designed motor should be analyzed and checked [34]. Comparing the PMA-SynRM to the PMSM, the rotor doesn't have winding loss since the rotor magnetic field is produced by magnets instead of rotor conductors [35]. However, to calculate the geometry of the motor it is necessary to determine its basic stator/rotor dimensions as given in Table 1.

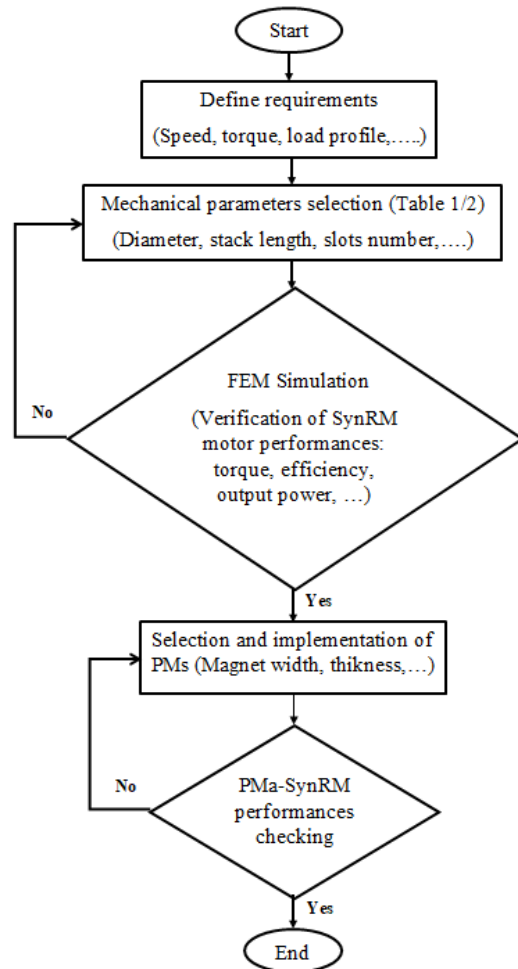


Fig. 3. Flowchart of design procedure

Table 1. Geometrical parameters of the motor

Parameter	Value
Stator Outer diameter	210 mm
Rotor outer diameter	147.3 mm
Air-gap length	0.7 mm
Stack length	150 mm
Number of stator slots	36

These dimensions are the stator and rotor dimensions and the motor stack length. The proposed PMA-SynRM stator and rotor 2-D cross section is shown in Fig.4. The PMA-SynRM stator has 36 slots with three-phase distributed windings and two pairs of pole. The rotor has four polyline flux barriers per pole and each barrier contains an inserted permanent magnet. Firstly, a SynRM with four flux barriers was designed and analyzed by Ansys-Maxwell. An optimal design of the flux barriers rotor is found using the parameters shown in Table 2.

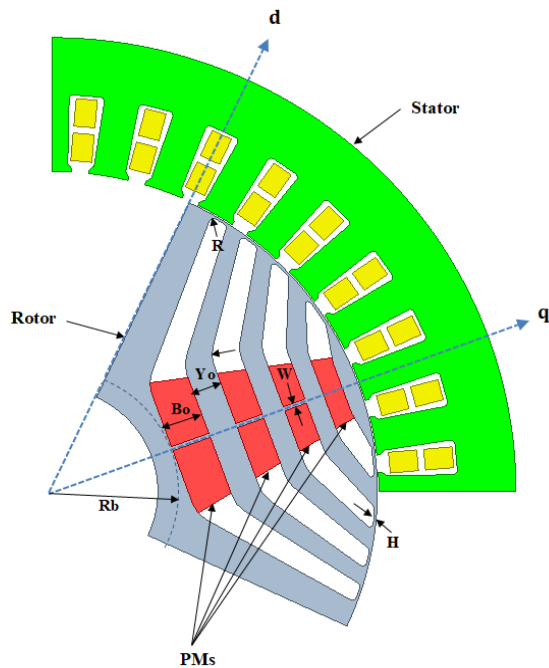


Fig. 4. One pole pitch view of the PMA-SynRM

The arc radius ( $R_b$ ) and flux-barrier width ( $B_o$ ) parameters affect the flux-barrier number and their emplacements and widths on the rotor, which affect the motor torque at the same time. The tangential rib ( $H$ ) and the radial rib ( $W$ ) can't be zero in the case of transversally laminated rotor because of mechanical reasons.

The SynRM performances were verified before the implementation of the PMs to the rotor barriers. The rotor pole magnets are selected as NdFe35 from the Maxwell library; and the steel sheet M16-24G is used for both stator and rotor core laminations.

Table 2. Parameters of the rotor flux barriers

Quantity & Symbol	Value
Tangential rib dimension ( $H$ )	0.5 mm
Radial rib dimension ( $W$ )	1 mm
Barrier fillet radius ( $R$ )	1 mm
Barrier arch center location ( $R_0$ )	7 mm
Incircle radius of the bottom barriers ( $R_b$ )	29 mm
Bottom width of the first barrier ( $B_o$ )	6.5 mm
Bottom width of the first tooth ( $Y_o$ )	9 mm

As a general procedure, while the motor is rotating at constant electrical speed ( $\omega=3000$  rpm) the back EMF is measured from the steady-state voltages. The air gap of the PMA-SynRM has a higher flux density which consequently leads to high back EMF amplitude. Fig.5 and Fig.6 illustrate the back EMF characteristic of the SynRM and the PMA-SynRM respectively.

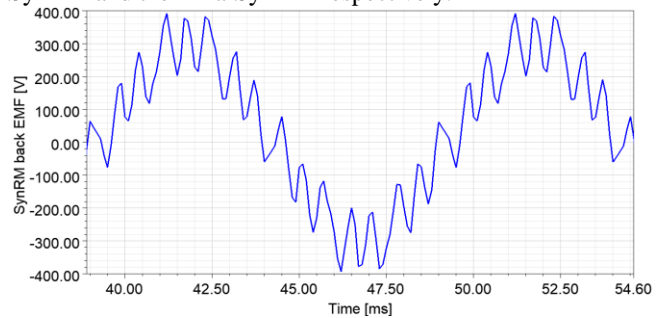


Fig. 5. Back EMF of SynRM

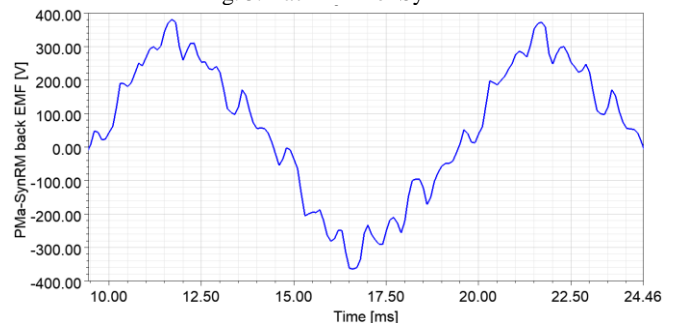


Fig. 6. Back EMF of PMA-SynRM

The back-EMF fundamental max-value for the PMA-SynRM topology is higher 41.27% than the SynRM topology back-EMF fundamental max-value.

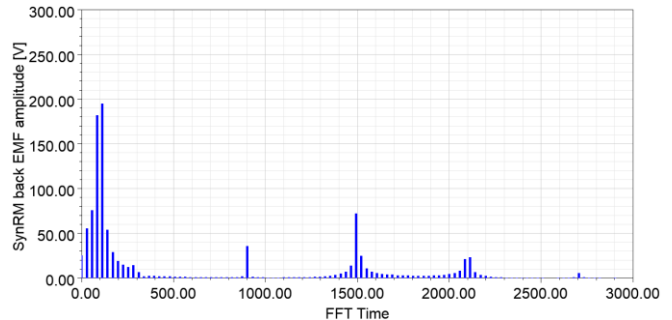


Fig. 7. Back EMF FFT of SynRM

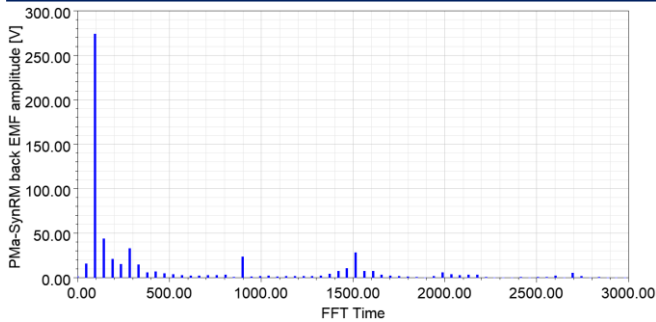


Fig. 8. Back EMF FFT of PMa-SynRM

Fast fourier transformer analysis illustrates the magnitude values of the first harmonic of the PMa-SynRM which is 16.15 volts as shown in Fig.7 and SynRM which is 55.82 volts as shown in Fig.8. Normally, if the number of stator slots increases the characteristic of the back EMF gets approximate to a sinusoidal wave [36,37].

The same geometries of both PMa-SynRM and SynRM are analyzed in FEM to show the accuracy of both models. The magnetic flux lines and flux densities are illustrated in Fig.9 and Fig.10. They show one magnetic pole of each machine in the quadrature position, so the magnetic flux passes through the flux barriers and PMs. It is clear that the flux lines are concentrated in PMa-SynRM because of the presence of PMs even though the density is importantly higher. In the designed model, PM width is reduced from the rotor to the stator, which affects the flux density distribution. After the implementation of the PMs, it is clear that torque density is higher compared to the conventional SynRM. Table 3 summarizes the difference between both motor topologies.

Table 3. Output parameters of SynRM and PMa-SynRM

Parameters	SynRM	PMa-SynRM
Torque average (Nm)	51.6	72
$L_d$ inductance (mH)	64.63	43.62
$L_q$ inductance (mH)	5.29	15.94
Output power (kW)	16.5	22.5
Efficiency	97.6%	99.4%

It is noticed that the PMa-SynRM strategy gives good results in terms of torque, and output power. Also the efficiency shows that the PF of the SynRM is lower. The assistance of PMs in the rotor flux barriers increases the saturation of the iron bridges as is shown in Fig.8. The flux linkage obtained by PMs compensates the flux  $L_q I_q$  and rotates the voltage vector towards the current vector, which reduces the angle  $\phi$  (Fig.1) and increases the PF.

#### 4. Field Oriented Control of PMa-SynRM

The FOC controller based on SVM technique made the PMa-SynRM simpler to use it in different applications [38], where the PMa-SynRM/Drive control structure is shown in Fig.11 and its parameters are illustrated in Table 4.

In this type of machines, d-q inductances are variable because of their dependency on self-axis current alongside the other axis current. Furthermore,  $L_d$  and  $L_q$  inductances are affected also by the position of the rotor comparable to the stator due to the variety of magnetic reluctance. Therefore, the PMa-SynRM rotor po-

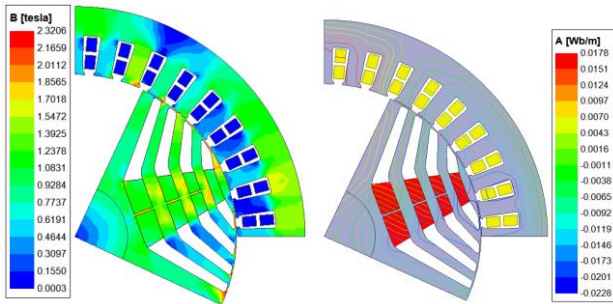


Fig. 9. Flux density and flux lines of PMa-SynRM

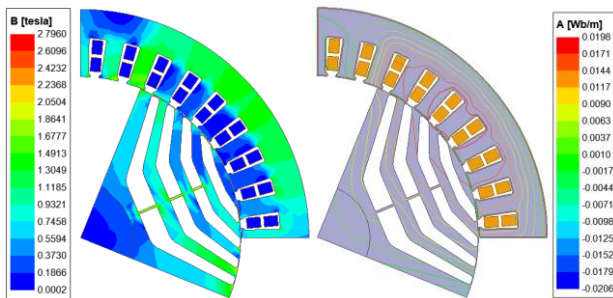


Fig. 10. Flux density and flux lines of SynRM

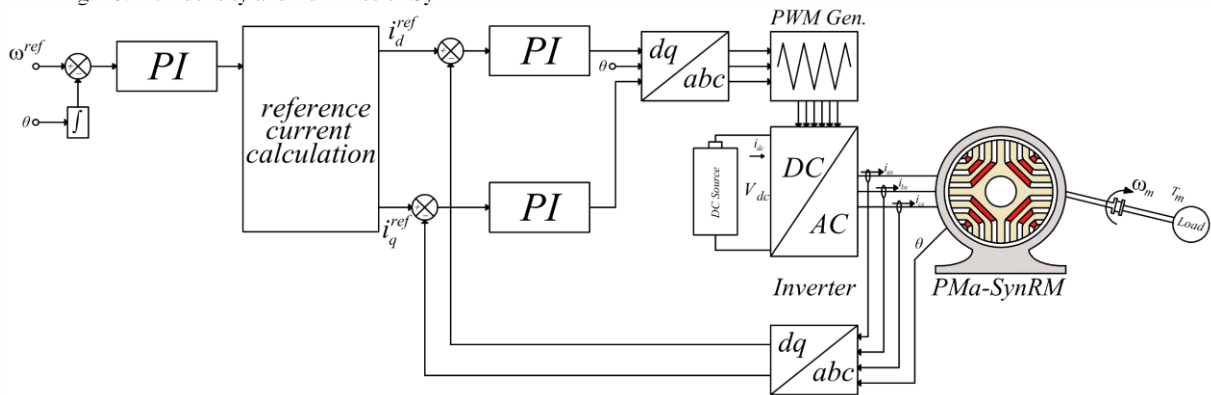


Fig. 11. FOC block diagram of the PMa-SynRM.

sition and the cross saturation are necessary for an exact representation of the motor control structure.

Table 4. PMA-SynRM/inverter and speed/current regulation parameters

Parameters	Values
pole pairs number	2
Stator resistance	0.75 Ω
$L_d$ inductance	43.62 mH
$L_q$ inductance	15.94 mH
Inertia coefficient	0.0188 Nm/(rad/s <sup>2</sup> )
Damping coefficient	0.01465 Nm/(rad/s)
Proportional gain of d-axis	96
Integral gain of d-axis	72
Proportional gain of q-axis	64
Integral gain of q-axis	72
Speed-proportional gain	32
Speed integral gain	128

The Current signals measured from the inverter output are transferred from a three-phase frame to the d-q frame. This transformation is based on the use of the flux angle. This angle is measured by an encoder and its value modified to velocity in the controller system.

The measured d-q currents ( $i_d-i_q$ ) are compared with currents reference ( $i_d^{ref}-i_q^{ref}$ ) and their error is controlled by tuned PI controllers in order to follow reference value. Finally, the back EMF and decoupling terms need to be compensated to produce the input SVM voltages.

Fig.12 shows the controller behavior of step variation in rotor speed from 1500 to 3000 rpm applied at a variable load condition. It is shown that the motor reaches the reference speed in 100 ms when a different load step applied and using PI controller. Fig. 13 shows the electromagnetic torque generated by the motor and the load torque when a step variation in load from 70 to 35 Nm is applied. Although the motor moves away from the reference value during the acceleration-deceleration periods, it is seen that it follows the reference value in steady state.

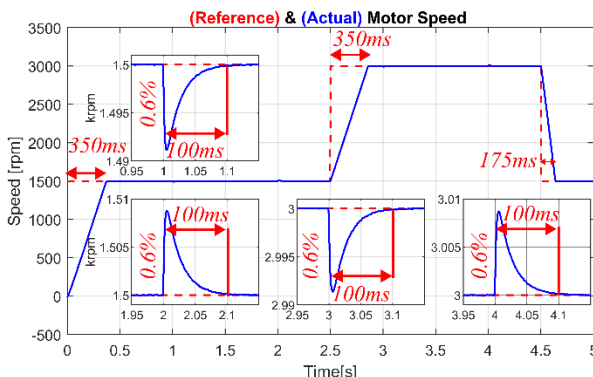


Fig. 12. Motor dynamic performances under different speed ranges

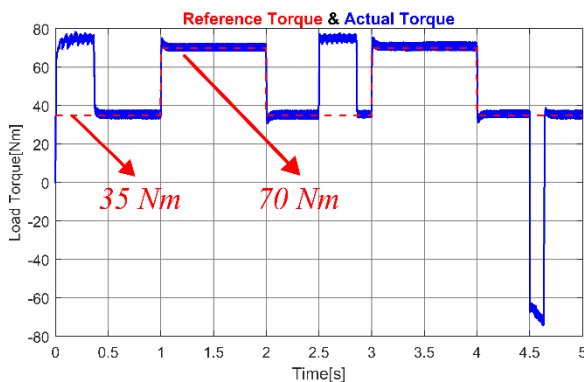


Fig. 13. Motor dynamic performances under variable load conditions



Fig. 14. Output power of the designed motor

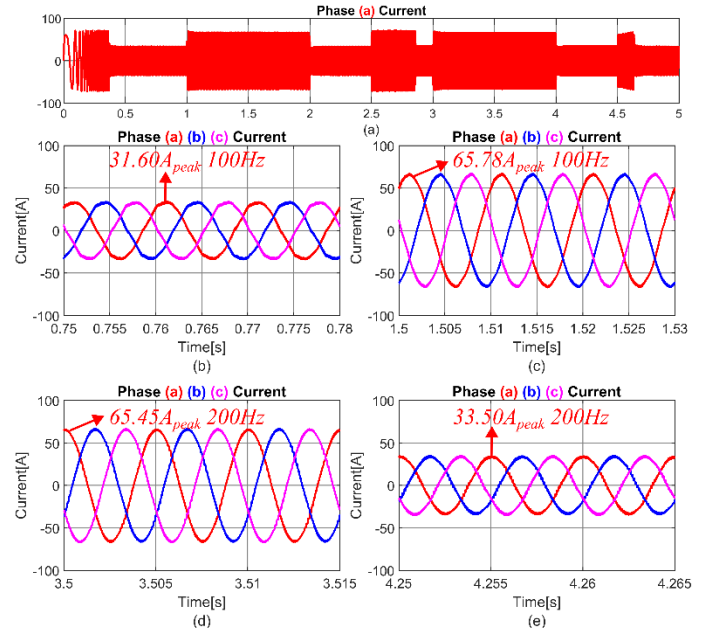


Fig. 15. Stator currents a) phase a current throughout the simulation b) phase currents at 30Nm load and 1500 rpm c) phase currents at 70Nm load and 1500 rpm d) phase currents at 70Nm load and 3000 rpm e) phase currents at 30Nm load and 3000 rpm

Fig. 14 shows the dynamic performances of the FOC control strategy under a closed-loop condition under variable load and

speed range conditions. Where (a) represents the output power of the motor, and (b) represents the three-phase currents wave form. These results demonstrate that the control system has a good robustness. Fig. 15 shows the phase currents at different load and speed values. Since the phase currents are in sinusoidal form throughout the simulation, it can be said that the designed motor operates stably and without vibration.

## 5. Conclusion

This work presents the design and the FOC control of PMA-SynRM motor using Ansys/Maxwell and MATLAB/Simulink software. The control schemes are detailed in the previous sections, where the motor system achieved good dynamic and steady-state performance and its robustness to the load and speed variations is improved. The simulation results of FE analysis validate the proposed PMA-SynRM motor design for the various performance parameters. An optimal solution was selected while designing a SynRM as maintained by the defined selection criterion after the selection of flux barriers parameters.

The optimal solution obtained was used for the implementation of PMs in the rotor barriers, which exhibits many benefits for the output performances of the PMA-SynRM:

- An increase of 39.5% in electromagnetic average torque and 36.4% in output power compared to SynRM.
- Minimization of back EMF harmonics and obtaining a high fundamental value which leads to 41.27%.
- The flux linkage obtained from PMs increases the flux density of the rotor, which increases the PF.

Hereafter, different starting points and more design parameters, including the optimization of PMs and the asymmetrical rotor topologies will be studied for the proposed PMA-SynRM/drive system.

## Conflict of Interest Statement

The authors declare that there is no conflict of interest in the study.

## CRedit Author Statement

**Loubna Boudjelida:** Formal analysis, Validation, Writing-original draft, **Cagdas Hisar:** Conceptualization, Validation, Data curation, Formal analysis, **Ibrahim Sefa:** Conceptualization, Supervision

## References

- [1] Hernandez M, Messagie M, Hegazy O, Marengo L, Winter O, Van Mierlo J. Environmental impact of traction electric motors for electric vehicles applications. *The International Journal of Life Cycle Assessment*. 2017;22(1):54-65.
- [2] J Gieras JF, Bianchi N. *Electric Motors for Light Traction*. EPE Journal. 2004;14(1):12-23.
- [3] Chung SU, Kim JW, Chun YD, Woo BC, Hong DK. Fractional Slot Concentrated Winding PMSM With Consequent Pole Rotor for a Low-Speed Direct Drive: Reduction of Rare Earth Permanent Magnet. *IEEE Transactions on Energy Conversion*. 2015;30(1):103-9.
- [4] Zhang Y, Xiang Z, Zhu X, Quan L, Jiang M. Anti-Demagnetization Capability Research of a Less-Rare-Earth Permanent-Magnet Synchronous Motor Based on the Modulation Principle. *IEEE Transactions on Magnetics*. 2021;57(2):1-6.
- [5] Musuroi S, Sorandaru C, Greconici M, Olarescu VN, Weinman M, editors. Low-cost ferrite permanent magnet assisted synchronous reluctance rotor an alternative solution for rare earth permanent magnet synchronous motors. *IECON 2013 - 39th Annual Conference of the IEEE Industrial Electronics Society*; 2013 10-13 Nov. 2013.
- [6] Tahanian H, Aliahmadi M, Faiz J. Ferrite Permanent Magnets in Electrical Machines: Opportunities and Challenges of a Non-Rare-Earth Alternative. *IEEE Transactions on Magnetics*. 2020;56(3):1-20.
- [7] Bonthu SSR, Arafat A, Choi S. Comparisons of Rare-Earth and Rare-Earth-Free External Rotor Permanent Magnet Assisted Synchronous Reluctance Motors. *IEEE Transactions on Industrial Electronics*. 2017;64(12):9729-38.
- [8] López Torres C. Analysis and implementation of a methodology for optimal PMA-SynRM design taking into account performances and reliability. Doctoral thesis, Universitat Politècnica de Catalunya, 2018.
- [9] Paltanea G, Paltanea VM, Hantila IF, Minciunescu P, Varaticeanu B, Demeter L, et al., editors. Numerical Analysis of a Free Rare-Earth PMA-SynRM for Light Electric Vehicle. *2021 International Conference on Applied and Theoretical Electricity (ICATE)*; 2021 27-29 May 2021.
- [10] Jani SN, Jamnani JG. A comparative study of electric motor for low-power density electric vehicles. *Environmental Science and Pollution Research*. 2023.
- [11] Mishra S, Nayak BK, Fernandes BG, editors. Parametric Design and Analysis of Ferrite PMA-SynRM for EV Application. *Smart Technologies for Power and Green Energy*; 2023; Singapore: Springer Nature Singapore.
- [12] Mohammadi A, Mirimani SM. Design of a Novel PM-Assisted Synchronous Reluctance Motor Topology Using V-Shape Permanent Magnets for Improvement of Torque Characteristic. *IEEE Transactions on Energy Conversion*. 2022;37(1):424-32.
- [13] Nobahari A, Vahedi A, Nasiri-Zarandi R. A Modified Permanent Magnet-Assisted Synchronous Reluctance Motor Design for Torque Characteristics Improvement. *IEEE Transactions on Energy Conversion*. 2022;37(2):989-98.
- [14] Mohanarajah T, Nagrial M, Rizk J, Hellany A. A Novel Method to Optimize Permanent Magnet Assisted Synchronous Reluctance Machines. *Electric Power Components and Systems*. 2020;48(9-10):933-43.
- [15] S Rafin SSM, Ali Q, Khan S, Lipo TA. A novel two-layer winding topology for sub-harmonic synchronous machines. *Electrical Engineering*. 2022;104(5):3027-35.
- [16] Ayub M, Hussain A, Jawad G, Kwon BI. Brushless Operation of a Wound-Field Synchronous Machine Using a Novel Winding Scheme. *IEEE Transactions on Magnetics*. 2019;55(6):1-4.

- [17]Jeong J, Lee H, Zapico MO, Lee SB, Reigosa DD, Blanco FBd, editors. Trailing Edge PM Demagnetization in Surface PM Synchronous Motors: Analysis and Detection. 2022 IEEE Energy Conversion Congress and Exposition (ECCE); 2022 9-13 Oct. 2022.
- [18]Ma Q, Refaie AE-, Fatemi A, editors. Multi-objective Design Optimization of a Blended Permanent Magnet Assisted Synchronous Reluctance Machine. 2021 IEEE International Electric Machines & Drives Conference (IEMDC); 2021 17-20 May 2021.
- [19]Wang J, Li Y, Wu S, Yu Z, Chen L. Analysis of the Influence of Parameter Condition on Whole Load Power Factor and Efficiency of Line Start Permanent Magnet Assisted Synchronous Reluctance Motor. *Energies* [Internet]. 2022; 15(11).
- [20]Guo H, He X, Xu J, Tian W, Sun G, Ju L, et al. Design of an Aviation Dual-Three-Phase High-Power High-Speed Permanent Magnet Assisted Synchronous Reluctance Starter-Generator With Antishort-Circuit Ability. *IEEE Transactions on Power Electronics*. 2022;37(10):12619-35.
- [21]Jammali YH, Mirzaeva G, Miller D, editors. Development of a PM-Assisted Synchronous Reluctance Motor Drive for an Electric Boat. 2020 Australasian Universities Power Engineering Conference (AUPEC); 2020 29 Nov.-2 Dec. 2020.
- [22]Dwivedi S, Tripathi SM, Sinha SK, editors. Review on Control Strategies of Permanent Magnet-Assisted Synchronous Reluctance Motor Drive. 2020 International Conference on Power Electronics & IoT Applications in Renewable Energy and its Control (PARC); 2020 28-29 Feb. 2020.
- [23]Kesler S, Kılıç A. Development of an Advanced AC Drive for the Heating Circulation Pumps with Dry-Rotor Using a Synchronous Reluctance Motor. *Electric Power Components and Systems*. 2023;51(16):1815-28.
- [24]Islam MK, Karimi-Ghartemani M, Choi S, editors. Design of a Robust Optimal Controller for Five-Phase Permanent Magnet Assisted Synchronous Reluctance Motor in Electric Vehicle Application. 2021 IEEE Applied Power Electronics Conference and Exposition (APEC); 2021 14-17 June 2021.
- [25]Sarkar P, Srinivas S, editors. MTPA based DTC for Permanent Magnet assisted Synchronous Reluctance Motor for Electric Vehicle application. 2019 IEEE Transportation Electrification Conference and Expo, Asia-Pacific (ITEC Asia-Pacific); 2019 8-10 May 2019.
- [26]Hua Y, Zhu H, Gao M, Ji Z. Multiobjective Optimization Design of Permanent Magnet Assisted Bearingless Synchronous Reluctance Motor Using NSGA- II . *IEEE Transactions on Industrial Electronics*. 2021;68(11):10477-87.
- [27]Degano M, Murataliyev M, Shuo W, Barater D, Buticchi G, Jara W, et al. Optimised Design of Permanent Magnet Assisted Synchronous Reluctance Machines for Household Appliances. *IEEE Transactions on Energy Conversion*. 2021;36(4):3084-95.
- [28]Qiu H, Zhang Y, Yang C, Yi R. Performance analysis and comparison of PMSM with concentrated winding and distributed winding. *Archives of Electrical Engineering*. 2023;69(2):303-17.
- [29]Mynarek P, Kołodziej J, Młot A, Kowol M, Łukaniszyn M. Influence of a Winding Short-Circuit Fault on Demagnetization Risk and Local Magnetic Forces in V-Shaped Interior PMSM with Distributed and Concentrated Winding. *Energies*. 2021; 14(16).
- [30]Tekgun D, Cosdu MM, Tekgun B, Alan I, editors. Investigation of the Effects of Multi-Layer Winding Structures in Two Pole Synchronous Reluctance Machines. 2021 3rd Global Power, Energy and Communication Conference (GPECOM); 2021 5-8 Oct. 2021.
- [31]Moallem M, Mirzaeian B, Mohammed OA, Lucas C. Multi-objective genetic-fuzzy optimal design of PI controller in the indirect field oriented control of an induction motor. *IEEE Transactions on Magnetics*. 2001;37(5):3608-12.
- [32]Lare P, Sarabi S, Delpha C, Nasr A, Diallo D, editors. Stator winding Inter-turn short-circuit and air gap eccentricity fault detection of a Permanent Magnet-Assisted Synchronous Reluctance Motor in Electrified vehicle. 2021 24th International Conference on Electrical Machines and Systems (ICEMS); 2021 31 Oct.-3 Nov. 2021.
- [33]Zamzoum O, El Mourabit Y, Errouha M, Derouich A, El Ghzizal A. Power control of variable speed wind turbine based on doubly fed induction generator using indirect field-oriented control with fuzzy logic controllers for performance optimization. *Energy Science & Engineering*. 2018;6(5):408-23.
- [34]Zhu X, Hua W, Wang W, Huang W. Analysis of Back-EMF in Flux-Reversal Permanent Magnet Machines by Air Gap Field Modulation Theory. *IEEE Transactions on Industrial Electronics*. 2019;66(5):3344-55.
- [35]Diao K, Sun X, Lei G, Guo Y, Zhu J. Multiobjective System Level Optimization Method for Switched Reluctance Motor Drive Systems Using Finite-Element Model. *IEEE Transactions on Industrial Electronics*. 2020;67(12):10055-64.
- [36]Zhao W, Xing F, Wang X, Lipo TA, Kwon Bi. Design and Analysis of a Novel PM-Assisted Synchronous Reluctance Machine With Axially Integrated Magnets by the Finite-Element Method. *IEEE Transactions on Magnetics*. 2017;53(6):1-4.
- [37]Hua W, Zhu X, Wu Z. Influence of Coil Pitch and Stator-Slot/Rotor-Pole Combination on Back EMF Harmonics in Flux-Reversal Permanent Magnet Machines. *IEEE Transactions on Energy Conversion*. 2018;33(3):1330-41.
- [38]Hyun D, Yun D, Baek J. Optimal Design of a Six-Phase Permanent-Magnet-Assisted Synchronous Reluctance Motor to Convert into Three Phases for Fault-Tolerant Improvement in a Traction System. *Applied Sciences*. 2021;11(18).